Int. J. Heat Mass Transfer. Vol. 36, No. 5, pp. 1147–1158, 1993
Printed in Great Britain

0017-9310/93 $6.00+0.00

Radiative transfer in a two-layer medium on a cylinder

CHIH-YANG WU and SHANG-CHEN WU
Department of Mechanical Engineering, National Cheng Kung University, Tainan, Taiwan 701, R.O.C.

(*Received* 6 *January* 1992 *and in final form* 9 *June* 1992)

Abstract—Radiative transfer in an absorbing and isotropically scattering two-layer medium around an opaque cylinder is considered. Numerical solutions of the integral equations of radiative transfer are obtained by the collocation method; differential approximation solutions are obtained by the spherical harmonics method. For most of the cases considered, reasonably accurate results can be obtained by using a four-term expansion for the integral equation method. The hemispherical–hemispherical and hemispherical–directional reflectivities of the medium exposed to diffuse radiation are presented. The effects of radius ratios, optical thicknesses and scattering albedos on the reflectivities are investigated. The outer layer of the medium has a great influence on the reflectivities.

1. INTRODUCTION

RADIATIVE heat transfer in multi-layer systems is of considerable interest in many applications because a large number of real objects under thermal radiation are systems consisting of several layers of absorbing and scattering materials. The systems include, among others, composite layers for thermal insulation, multi-layer glass windows in a solar collector, atmospheres and laminated biotissues. Numerous methods for studying the problem have been reported. Iliasov and Krasnikov [1] used the two-flux method to study selective absorption and scattering in multi-layer media. Devaux *et al.* [2] used the P-*N* method to solve the radiative transfer problem, based on the general anisotropically scattering model, in multi-layer atmospheres. The F-*N* method was also applied to obtain the transmissivity and reflectivity of an isotropically scattering two-layer slab with diffusely and specularly reflecting boundaries by Shouman and Özisik [3] and those of a multi-layer slab by Clements and Özisik [4]. Radiative heat transfer in a two-layer slab was also solved by expanding the source function in the integral form of the equation of radiative transfer [5]. Stamnes and Conklin [6] applied the discrete ordinate method to radiative transfer in multi-layer atmospheres. Reflectivity of a two-layer slab with linear-anisotropic scattering has been obtained by the P-11 approximation [7]. Moreover, the problems of radiative transfer through multi-layer coatings and glass windows have been studied extensively in the literature (e.g. see ref. [8] for a detailed bibliography). Recently, a few works considered multi-dimensional problems [9, 10] and the interaction of heat conduction and radiation in multi-layer media [11, 12]. The previous analyses studied almost every aspect of the problems. However, only brief attention [10] was paid to the problems in cylindrical geometry.

In contrast to most of the previous analyses, the present work considers radiative transfer in a two-layer medium around an opaque cylinder. The two layers considered may have different scattering and absorption coefficients. The problems of radiative transfer in a one-dimensional single-layer cylindrical medium have been studied extensively in the literature [13–19]. Examples of solution methods to radiation transfer in cylindrical geometry are the Monte Carlo method [13], the variational method [14], the differential approximation [15], the source function expansion [16–18] and the discrete ordinate method [19]. It has been shown that the results obtained by solving the exact integral equations of radiative transfer are highly accurate [5, 16–18], while the spherical harmonics method [7, 15] takes little computational time to generate reasonably good results for large scattering albedos or optical thicknesses. Thus, these two methods are adopted. In the present work, the integral equations of radiative transfer in a two-layer medium are derived and the method of collocation is utilized for solutions; the solutions of the differential approximation are obtained by the finite difference method. The results obtained by the two methods are compared. Comparisons of results by the present methods and those by the F-*N* method [4] and the P-11 approximation [7] for planar media are also made. The reflectivity, one of the most important apparent properties, is presented and discussed for a wide range of parameters, including the radius ratio, the optical thickness and the scattering albedo.

2. ANALYSIS

The basic assumptions about the system in which the radiative transfer takes place are: (a) the medium is absorbing and isotropically scattering; (b) the

NOMENCLATURE

- $C_{i,j}$ expansion coefficients for layer i in equation (18)
- D_1 radius ratio, r_1/r_0
- D_2 radius ratio, r_2/r_0
- $I_i(r, \theta, \phi)$ radiation intensity for layer i
- $I_{ic}(r, \theta, \phi)$ component of the intensity due to the attenuated incident intensity along the path of the beam
- $I_{im}(r, \theta, \phi)$ component of the intensity due to the radiation scattered by the medium into the path of the beam
- $I_{i,n}(r)$ functions defined by equation (20)
- $I_{0,i}$ incident intensity
- J_i number of expansion terms for layer i
- $K_{i_n}(y)$ Bickley functions defined by equation (13)
- N order of the P-N approximations
- $q_2^+(r_2)$ exit radiative flux at $r = r_2$
- $q_{2c}^+(r_2)$ component of $q_2^+(r_2)$, see equation (16a)
- $q_{2m}^+(r_2)$ component of $q_2^+(r_2)$, see equation (16b)
- R hemispherical–hemispherical reflectivity
- R_c component of R, $R_c = q_{2c}^+(r_2)$
- R_m component of R, $R_m = q_{2m}^+(r_2)$
- $r_{i,k}$ collocation points for layer i
- r_0, r_1, r_2 geometrical radii
- $S_i(r)$ source function for layer i
- s path along the beam
- $s_n(r, r', \phi')$ function defined by equation (10)
- $s_r^\pm(r, r', \phi')$ functions defined by equation (11)
- $s_0^\pm(r, r', \theta, \phi)$ functions defined by equation (6)
- $x(r, r', \phi)$ function defined by equation (7)
- y variable utilized in equation (13).

Greek symbols

- α integration variable utilized in equations (8) and (16)
- β_i extinction coefficient for layer i
- η angle (see Fig. 1(a))
- θ polar angle
- ξ angle (see Fig. 1(a))
- ρ_θ hemispherical–directional reflectivity
- $\rho_{\theta c}$ component of ρ_θ due to the attenuated incident intensity along the path of the beam
- $\rho_{\theta m}$ component of ρ_θ due to the radiation scattered by the medium into the path of the beam
- τ_1 optical thickness of layer 1, $\beta_1(r_1 - r_0)$
- τ_2 optical thickness of layer 2, $\beta_2(r_2 - r_1)$
- ϕ azimuthal angle
- $\psi(r, r')$ functions defined by equation (9)
- ω_i scattering albedo for layer i.

Subscripts

- i 1 or 2, referring to layer 1 and layer 2, respectively
- k collocation points
- n order of $I_{i,n}(r)$ defined by equation (20).

physical properties of the medium are constant; (c) the boundaries of the medium and the interface between the two layers are nonreflecting; (d) the outer boundary with radius r_2 is exposed to diffuse and cylindrically symmetric radiation and the inner boundary with radius r_0 is opaque; (e) the geometrical dimension of the layers is much greater than one wavelength. The geometry and coordinates are shown in Fig. 1(a). For cylindrical symmetry, the equations of radiative transfer are given as

$$\sin\theta\left[\cos\phi\frac{\partial I_i}{\partial r} - \frac{\sin\phi}{r}\frac{\partial I_i}{\partial \phi}\right] + \beta_i I_i = \beta_i S_i, \quad i = 1, 2. \tag{1}$$

Here, I_i denotes the radiation intensity nondimensionalized by the incident radiation intensity, r the geometrical variable in the radial direction, θ the polar angle, ϕ the azimuthal angle, β_i the extinction coefficient for layer i, and S_i the source function defined by

$$S_i(r) = \frac{\omega_i}{4\pi}\int_{\theta=0}^{\pi}\int_{\phi=0}^{2\pi} I_i(r, \theta, \phi)\sin\theta \, d\phi \, d\theta,$$

$$i = 1, 2 \tag{2}$$

where ω_i is the scattering albedo. In the present work, the inner and outer layers are denoted by layers 1 and 2, respectively.

The boundary conditions for equation (1) can be written as

$$I_1(r_0, \theta, \phi) = I_{0,1},$$
$$0 \leqslant \theta \leqslant \pi, \quad -\pi/2 \leqslant \phi \leqslant \pi/2 \tag{3a}$$

$$I_2(r_2, \theta, \phi) = I_{0,2},$$
$$0 \leqslant \theta \leqslant \pi, \quad \pi/2 \leqslant \phi \leqslant 3\pi/2 \tag{3b}$$

$$I_1(r_1, \theta, \phi) = I_2(r_1, \theta, \phi),$$
$$0 \leqslant \theta \leqslant \pi, \quad -\pi/2 \leqslant \phi \leqslant \pi/2 \tag{3c}$$

$$I_1(r_1, \theta, \phi) = I_2(r_1, \theta, \phi),$$
$$0 \leqslant \theta \leqslant \pi, \quad \pi/2 \leqslant \phi \leqslant 3\pi/2 \tag{3d}$$

where r_1 and r_2 are the radii shown in Fig. 1(b), and $I_{0,1}$ and $I_{0,2}$ are the incident intensities at $r = r_0$ and

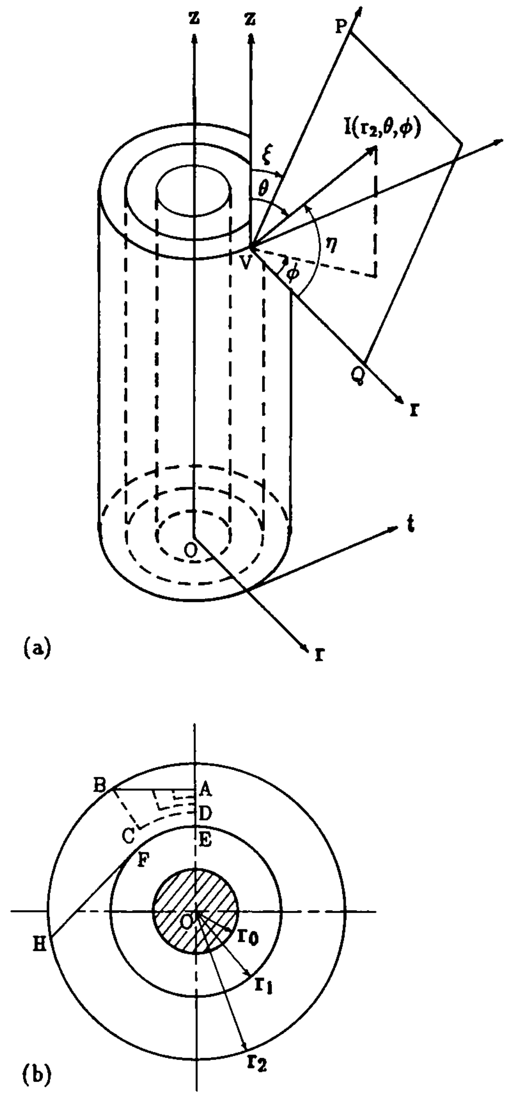

FIG. 1. Geometry and coordinates (a) and partition of the integration domain (b).

$r = r_2$, respectively. In this work, the values of $I_{0,1}$ and $I_{0,2}$ are considered as 0 and $1/\pi$, respectively.

2.1. *Integral equations of transfer*

Following the procedure described in refs. [8, 20], the formal solution of the intensity is found to be

$$\begin{aligned} I_1(r,\theta,\phi) &= I_{0,1}\exp[-\beta_1 s_0^-(r,r_0,\theta,\phi)] \\ &\quad + \int_0^{s_0^-(r,r_0,\theta,\phi)} S_1[x(r,s\sin\theta,\phi)]\exp(-\beta_1 s)\beta_1\,\mathrm{d}s, \\ &\qquad 0 \leqslant \theta \leqslant \pi, \quad 0 \leqslant \phi \leqslant \sin^{-1}(r_0/r) \qquad \text{(4a)} \\ &= I_{0,2}\exp\{-\beta_1 s_0^+(r,r_1,\theta,\phi) - \beta_2[s_0^+(r,r_2,\theta,\phi) \\ &\quad - s_0^+(r,r_1,\theta,\phi)]\} + \int_0^{s_0^+(r,r_1,\theta,\phi)} S_1[x(r,s\sin\theta,\phi)] \\ &\quad \times \exp(-\beta_1 s)\beta_1\,\mathrm{d}s + \int_{s_0^+(r,r_1,\theta,\phi)}^{s_0^+(r,r_2,\theta,\phi)} S_2[x(r,s\sin\theta,\phi)] \\ &\quad \times \exp\{-\beta_1 s_0^+(r,r_1,\theta,\phi) \\ &\quad -\beta_2[s-s_0^+(r,r_1,\theta,\phi)]\}\beta_2\,\mathrm{d}s, \\ &\qquad 0 \leqslant \theta \leqslant \pi, \quad \sin^{-1}(r_0/r) \leqslant \phi \leqslant \pi \qquad \text{(4b)} \end{aligned}$$

$$\begin{aligned} I_2(r,\theta,\phi) &= I_{0,1}\exp\{-\beta_2 s_0^-(r,r_1,\theta,\phi) \\ &\quad -\beta_1[s_0^-(r,r_0,\theta,\phi) \\ &\quad -s_0^-(r,r_1,\theta,\phi)]\} + \int_0^{s_0^-(r,r_1,\theta,\phi)} S_2[x(r,s\sin\theta,\phi)] \\ &\quad \times\exp(-\beta_2 s)\beta_2\,\mathrm{d}s + \int_{s_0^-(r,r_1,\theta,\phi)}^{s_0^-(r,r_0,\theta,\phi)} S_1[x(r,s\sin\theta,\phi)] \\ &\quad \times\exp\{-\beta_2 s_0^-(r,r_1,\theta,\phi) \\ &\quad -\beta_1[s-s_0^-(r,r_1,\theta,\phi)]\}\beta_1\,\mathrm{d}s, \\ &\qquad 0 \leqslant \theta \leqslant \pi, \quad 0 \leqslant \phi \leqslant \sin^{-1}(r_0/r) \qquad \text{(5a)} \\ &= I_{0,2}\exp\{-\beta_2 s_0^-(r,r_1,\theta,\phi) - \beta_1[s_0^+(r,r_1,\theta,\phi) \\ &\quad -s_0^-(r,r_1,\theta,\phi)] - \beta_2[s_0^+(r,r_2,\theta,\phi) \\ &\quad -s_0^+(r,r_1,\theta,\phi)]\} \\ &\quad + \int_0^{s_0^-(r,r_1,\theta,\phi)} S_2[x(r,s\sin\theta,\phi)]\exp(-\beta_2 s)\beta_2\,\mathrm{d}s \\ &\quad + \int_{s_0^-(r,r_1,\theta,\phi)}^{s_0^+(r,r_1,\theta,\phi)} S_1[x(r,s\sin\theta,\phi)] \\ &\quad \times\exp\{-\beta_2 s_0^-(r,r_1,\theta,\phi) \\ &\quad -\beta_1[s-s_0^-(r,r_1,\theta,\phi)]\}\beta_1\,\mathrm{d}s \\ &\quad + \int_{s_0^+(r,r_1,\theta,\phi)}^{s_0^+(r,r_2,\theta,\phi)} S_2[x(r,s\sin\theta,\phi)]\exp\{-\beta_2 s_0^-(r,r_1,\theta,\phi) \\ &\quad -\beta_1[s_0^+(r,r_1,\theta,\phi)-s_0^-(r,r_1,\theta,\phi)] \\ &\quad -\beta_2[s-s_0^+(r,r_1,\theta,\phi)]\}\beta_2\,\mathrm{d}s, \\ &\qquad 0 \leqslant \theta \leqslant \pi, \quad \sin^{-1}(r_0/r) \leqslant \phi \leqslant \sin^{-1}(r_1/r) \qquad \text{(5b)} \\ &= I_{0,2}\exp[-\beta_2 s_0^+(r,r_2,\theta,\phi)] \\ &\quad + \int_0^{s_0^+(r,r_2,\theta,\phi)} S_2[x(r,s\sin\theta,\phi)]\exp(-\beta_2 s)\beta_2\,\mathrm{d}s, \\ &\qquad 0 \leqslant \theta \leqslant \pi, \quad \sin^{-1}(r_1/r) \leqslant \phi \leqslant \pi \qquad \text{(5c)} \end{aligned}$$

where functions $s_0^{\pm}(r,r',\theta,\phi)$ and $x(r,r',\phi)$ are defined as

$$s_0^{\pm}(r,r',\theta,\phi) = (r\cos\phi \pm \sqrt{(r'^2 - r^2\sin^2\phi)})\operatorname{cosec}\theta \qquad (6)$$

$$x(r,r',\phi) = \sqrt{(r^2 + r'^2 - 2rr'\cos\phi)} \qquad (7)$$

and s is the path along the beam. The intensity $I_i(r,\theta,\phi)$ can be split into two components, $I_{ic}(r,\theta,\phi)$, which equals the first term of the RHS (equations (4) and (5)) due to the attenuated incident intensity along the path of the beam, and $I_{im}(r,\theta,\phi)$, which includes the rest of the terms of the RHS (equations (4) and (5)) due to the radiation scattered by the medium into the path of the beam. Substituting equations (4) and (5) into equation (2), the integral equations for the source functions are obtained as

$$
\begin{aligned}
S_1(r) = {} & \frac{\omega_1}{\pi}\int_{r_0}^{r_1}\int_{\alpha'=\psi(r,r')}^{\cos^{-1}(r_0/r)+\cos^{-1}(r_0/r')} S_1(r') \\
& \times K_{i_1}[\beta_1 s_n(r,r',\phi')]\frac{\beta_1 r'\,\mathrm{d}\alpha'\,\mathrm{d}r'}{x(r,r',\alpha')} \\
& + \frac{\omega_1}{\pi}\int_{r}^{r_1}\int_{\alpha'=0}^{\psi(r,r')} S_1(r')K_{i_1}[\beta_1 s_n(r,r',\phi')]\frac{\beta_1 r'\,\mathrm{d}\alpha'\,\mathrm{d}r'}{x(r,r',\alpha')} \\
& + \frac{\omega_1}{\pi}\int_{r_1}^{r_2}\int_{\alpha'=0}^{\cos^{-1}(r_0/r)+\cos^{-1}(r_0/r')} S_2(r')K_{i_1}\{\beta_1 s_r^+(r,r_1,\phi') \\
& + \beta_2[s_r^+(r,r',\phi')-s_r^+(r,r_1,\phi')]\}\frac{\beta_2 r'\,\mathrm{d}\alpha'\,\mathrm{d}r'}{x(r,r',\alpha')} \\
& + \frac{\omega_1}{\pi^2}\int_{\alpha'=0}^{\cos^{-1}(1/D_2)+\cos^{-1}(r_0/r)} K_{i_2}\{\beta_1 s_r^+(r,r_1,\phi') \\
& + \beta_2[s_r^+(r,r_2,\phi')-s_r^+(r,r_1,\phi')]\}(r_2-r\cos\alpha') \\
& \times \frac{r_2\,\mathrm{d}\alpha'}{x^2(r,r_2,\alpha')}
\end{aligned}
\tag{8a}
$$

$$
\begin{aligned}
S_2(r) = {} & \frac{\omega_2}{\pi}\int_{r_0}^{r_1}\int_{\alpha'=0}^{\cos^{-1}(r_0/r)+\cos^{-1}(r_0/r')} S_1(r') \\
& \times K_{i_1}[\beta_1 s_n(r,r',\phi')]\frac{\beta_1 r'\,\mathrm{d}\alpha'\,\mathrm{d}r'}{x(r,r',\alpha')} \\
& + \frac{\omega_2}{\pi}\int_{r_1}^{r_2}\int_{\alpha'=\psi(r,r')}^{\cos^{-1}(r_1/r)+\cos^{-1}(r_1/r')} S_2(r') \\
& \times K_{i_1}[\beta_2 s_n(r,r',\phi')]\frac{\beta_2 r'\,\mathrm{d}\alpha'\,\mathrm{d}r'}{x(r,r',\alpha')} \\
& + \frac{\omega_2}{\pi}\int_{r}^{r_2}\int_{\alpha'=0}^{\psi(r,r')} S_2(r') \\
& \times K_{i_1}[\beta_2 s_n(r,r',\phi')]\frac{\beta_2 r'\,\mathrm{d}\alpha'\,\mathrm{d}r'}{x(r,r',\alpha')} \\
& + \frac{\omega_2}{\pi}\int_{r_1}^{r_2}\int_{\cos^{-1}(r_1/r)+\cos^{-1}(r_1/r')}^{\cos^{-1}(r_0/r)+\cos^{-1}(r_0/r')} S_2(r')K_{i_1}\{\beta_2 s_r^-(r,r_1,\phi') \\
& + \beta_1[s_r^+(r,r_1,\phi')-s_r^-(r,r_1,\phi')] \\
& + \beta_2[s_r^+(r,r',\phi')-s_r^+(r,r_1,\phi')]\}\frac{\beta_2 r'\,\mathrm{d}\alpha'\,\mathrm{d}r'}{x(r,r',\alpha')} \\
& + \frac{\omega_2}{\pi^2}\int_{\alpha'=0}^{\cos^{-1}(D_1/D_2)+\cos^{-1}(r_1/r)} K_{i_2}[\beta_2 s_r^+(r,r_2,\phi')] \\
& \times (r_2-r\cos\alpha')\frac{r_2\,\mathrm{d}\alpha'}{x^2(r,r_2,\alpha')} \\
& + \frac{\omega_2}{\pi^2}\int_{\cos^{-1}(D_1/D_2)+\cos^{-1}(r_1/r)}^{\cos^{-1}(1/D_2)+\cos^{-1}(r_0/r)} K_{i_2}\{\beta_2 s_r^-(r,r_1,\phi') \\
& + \beta_1[s_r^+(r,r_1,\phi')-s_r^-(r,r_1,\phi')] + \beta_2[s_r^+(r,r_2,\phi') \\
& - s_r^+(r,r_1,\phi')]\}(r_2-r\cos\alpha')\frac{r_2\,\mathrm{d}\alpha'}{x^2(r,r_2,\alpha')}.
\end{aligned}
\tag{8b}
$$

In equations (8a) and (8b)

$$
\psi(r,r') = \begin{cases} \cos^{-1}(r/r'), & \text{for } r' > r \\ 0, & \text{for } r' \leqslant r \end{cases}
\tag{9}
$$

$$
s_n(r,r',\phi') =
$$

$$
\begin{cases} s_r^+(r,r',\phi'), & \text{for } r' \leqslant r,\quad \alpha' > \cos^{-1}(r'/r) \text{ or } r' > r \\ s_r^-(r,r',\phi'), & \text{for } r' \leqslant r,\quad \alpha' \leqslant \cos^{-1}(r'/r) \end{cases}
\tag{10}
$$

$$
s_r^{\pm}(r,r',\phi') = s_0^{\pm}(r,r',\pi/2,\phi')
\tag{11}
$$

$$
\phi' = \begin{cases} \sin^{-1}[r'\sin\alpha'/x(r,r',\alpha')], \\ \quad \text{for } r' > r,\quad \alpha' > \cos^{-1}(r/r') \text{ or } r' \leqslant r \\ \pi - \sin^{-1}[r'\sin\alpha'/x(r,r',\alpha')], \\ \quad \text{for } r' > r,\quad \alpha' \leqslant \cos^{-1}(r/r'). \end{cases}
\tag{12}
$$

$K_{i_n}(y)$ is the so-called Bickley function, defined as

$$
K_{i_n}(y) = \int_1^{\infty}\frac{\exp(-yt)}{t^n\sqrt{(t^2-1)}}\,\mathrm{d}t,\quad n = 1,2,\ldots
\tag{13}
$$

and D_1 and D_2 are the radius ratios defined as

$$
D_1 = r_1/r_0
\tag{14a}
$$

$$
D_2 = r_2/r_0.
\tag{14b}
$$

Similarly, the exit radiative flux at $r = r_2$ can be expressed as

$$
q_2^+(r_2) = q_{2\mathrm{c}}^+(r_2) + q_{2\mathrm{m}}^+(r_2)
\tag{15}
$$

where

$$
\begin{aligned}
q_{2\mathrm{c}}^+(r_2) = {} & \frac{4}{\pi}\int_{\alpha'=0}^{2\cos^{-1}(D_1/D_2)} (r_2 - r_2\cos\alpha') \\
& \times K_{i_3}[\beta_2 s_r^+(r_2,r_2,\phi')](r_2-r_2\cos\alpha')\frac{r_2\,\mathrm{d}\alpha'}{x^3(r_2,r_2,\alpha')} \\
& + \frac{4}{\pi}\int_{2\cos^{-1}(D_1/D_2)}^{2\cos^{-1}(1/D_2)} (r_2-r_2\cos\alpha')K_{i_3}\{\beta_2 s_r^-(r_2,r_1,\phi') \\
& + \beta_1[s_r^+(r_2,r_1,\phi')-s_r^-(r_2,r_1,\phi')] \\
& + \beta_2[s_r^+(r_2,r_2,\phi')-s_r^+(r_2,r_1,\phi')]\}(r_2-r_2\cos\alpha') \\
& \times \frac{r_3\,\mathrm{d}\alpha'}{x^3(r_2,r_2,\alpha')}
\end{aligned}
\tag{16a}
$$

$$
\begin{aligned}
q_{2\mathrm{m}}^+(r_2) = {} & 4\int_{r_0}^{r_1}\int_{\alpha'=0}^{\cos^{-1}(1/D_2)+\cos^{-1}(r_0/r')} (r_2 - r'\cos\alpha')S_1(r') \\
& \times K_{i_2}[\beta_1 s_n(r_2,r',\phi')]\frac{\beta_1 r'\,\mathrm{d}\alpha'\,\mathrm{d}r'}{x^2(r_2,r',\alpha')} \\
& + 4\int_{r_1}^{r_2}\int_{\alpha'=0}^{\cos^{-1}(D_1/D_2)+\cos^{-1}(r_1/r')} (r_2 - r'\cos\alpha')S_2(r')
\end{aligned}
$$

$$\times K_{i_2}[\beta_2 s_n(r_2, r', \phi')] \frac{\beta_2 r' \,\mathrm{d}\alpha' \,\mathrm{d}r'}{x^2(r_2, r', \alpha')}$$

$$+4 \int_{r_1}^{r_2} \int_{\cos^{-1}(D_1/D_2)+\cos^{-1}(r_1/r')}^{\cos^{-1}(1/D_2)+\cos^{-1}(r_0/r')} (r_2 - r' \cos\alpha') S_2(r')$$

$$\times K_{i_2}\{\beta_2 s_r^-(r_2, r_1, \phi') + \beta_1 [s_r^+(r_2, r_1, \phi')$$

$$- s_r^-(r_2, r_1, \phi')] + \beta_2 [s_r^+(r_2, r', \phi') - s_r^+(r_2, r_1, \phi')]\}$$

$$\times \frac{\beta_2 r' \,\mathrm{d}\alpha' \,\mathrm{d}r'}{x^2(r_2, r', \alpha')}. \tag{16b}$$

Moreover, the hemispherical–hemispherical reflectivity is defined by

$$R = R_c + R_m \tag{17}$$

where R_c represents the contribution of the attenuated incident radiation, i.e. $q_{2c}^+(r_2)$, and R_m represents the contribution of the scattered radiation by the medium, i.e. $q_{2m}^+(r_2)$. After solving equations (8a) and (8b), the radiative intensity can be obtained by substituting $S_1(r)$ and $S_2(r)$ into equations (4) and (5). The hemispherical–directional reflectivity, ρ_θ, is equal to $I_2(r_2, \theta, \phi)$, where $0 \leqslant \theta \leqslant \pi$, $-\pi/2 \leqslant \phi \leqslant \pi/2$. Similar to the intensity, ρ_θ can be separated as $\rho_{\theta c} = I_{2c}(r_2, \theta, \phi)$ and $\rho_{\theta m} = I_{2m}(r_2, \theta, \phi)$.

2.2. *Application of the collocation method to the integral equations*

To solve the simultaneous integral equations for $S_1(r)$ and $S_2(r)$, the collocation method is used. Here, we represent $S_1(r)$ and $S_2(r)$ in terms of the Lagrange polynomials as

$$S_1(r) = \sum_{j=1}^{J_1} C_{1,j} \prod_{\substack{k=1 \\ k \neq j}}^{J_1} (r - r_{1,k})/(r_{1,j} - r_{1,k}),$$

$$r_0 < r < r_1 \tag{18a}$$

and

$$S_2(r) = \sum_{j=1}^{J_2} C_{2,j} \prod_{\substack{k=1 \\ k \neq j}}^{J_2} (r - r_{2,k})/(r_{2,j} - r_{2,k}),$$

$$r_1 < r < r_2 \tag{18b}$$

where $C_{1,j}$ and $C_{2,j}$ denote unknown expansion coefficients, $r_{1,k}$ and $r_{2,k}$ denote collocation points, and Π is the product symbol. Substituting equations (18a) and (18b) into equations (8a) and (8b) and forcing the RHS = LHS at a set of collocation points yields a system of $(J_1 + J_2)$ algebraic equations for an equal number of unknown expansion coefficients, provided that all integrations in equations (8a) and (8b) can be finished. Since some of the integrations are over domains with singularities, the partition–extrapolation technique [18, 21] is adopted to overcome the difficulty. The technique is illustrated in the Appendix. For the accuracy of the numerical results, the zeros of the Chebyshev polynomials [22] are chosen as the collocation points.

Once these expansion coefficients are determined, the hemispherical–hemispherical reflectivity can be obtained by substituting equations (18a) and (18b) into equations (15) and (17), while the hemispherical–directional reflectivity can be obtained by substituting equations (18a) and (18b) into the formal solution of the intensity and the definition of ρ_θ.

2.3. *P-N approximations*

The spherical harmonics method [8, 15] is also used to solve the present problem. The P-11 approximation to the present problem is the following:

$$\frac{\mathrm{d}I_{i,0}}{\mathrm{d}r} = \frac{193\,618}{3465r} I_{i,0} - 78\beta_i I_{i,1} - \frac{1910}{r} I_{i,2}$$

$$+ 975\beta_i I_{i,3} + \frac{12\,878}{r} I_{i,4} - 4420\beta_i I_{i,5}$$

$$- \frac{495\,014}{15r} I_{i,6} + \frac{62\,985}{7} \beta_i I_{i,7} + \frac{251\,498}{7r} I_{i,8}$$

$$- 8398\beta_i I_{i,9} - \frac{41\,990}{3r} I_{i,10} + \frac{96\,577}{33} \beta_i I_{i,11} \tag{19a}$$

$$\frac{\mathrm{d}I_{i,1}}{\mathrm{d}r} = (\omega_i - 1)\beta_i I_{i,0} - \frac{1}{r} I_{i,1} \tag{19b}$$

$$\frac{\mathrm{d}I_{i,2}}{\mathrm{d}r} = \frac{2}{3r} I_{i,0} - \beta_i I_{i,1} - \frac{2}{r} I_{i,2} \tag{19c}$$

$$\frac{\mathrm{d}I_{i,3}}{\mathrm{d}r} = \frac{1}{3}\omega_i \beta_i I_{i,0} + \frac{8}{5r} I_{i,1} - \beta_i I_{i,2} - \frac{3}{r} I_{i,3} \tag{19d}$$

$$\frac{\mathrm{d}I_{i,4}}{\mathrm{d}r} = -\frac{2}{35r} I_{i,0} + \frac{18}{7r} I_{i,2} - \beta_i I_{i,3} - \frac{4}{r} I_{i,4} \tag{19e}$$

$$\frac{\mathrm{d}I_{i,5}}{\mathrm{d}r} = \frac{1}{5}\omega_i \beta_i I_{i,0} - \frac{8}{105r} I_{i,1} + \frac{32}{9r} I_{i,3} - \beta_i I_{i,4} - \frac{5}{r} I_{i,5} \tag{19f}$$

$$\frac{\mathrm{d}I_{i,6}}{\mathrm{d}r} = -\frac{16}{693r} I_{i,0} - \frac{20}{231r} I_{i,2} + \frac{50}{11r} I_{i,4} - \beta_i I_{i,5} - \frac{6}{r} I_{i,6} \tag{19g}$$

$$\frac{\mathrm{d}I_{i,7}}{\mathrm{d}r} = \frac{1}{7}\omega_i \beta_i I_{i,0} - \frac{32}{1001r} I_{i,1}$$

$$- \frac{40}{429r} I_{i,3} + \frac{72}{13r} I_{i,5} - \beta_i I_{i,6} - \frac{7}{r} I_{i,7} \tag{19h}$$

$$\frac{\mathrm{d}I_{i,8}}{\mathrm{d}r} = -\frac{16}{1287r} I_{i,0} - \frac{16}{429r} I_{i,2}$$

$$- \frac{14}{143r} I_{i,4} + \frac{98}{15r} I_{i,6} - \beta_i I_{i,7} - \frac{8}{r} I_{i,8} \tag{19i}$$

$$\frac{\mathrm{d}I_{i,9}}{\mathrm{d}r} = \frac{1}{9}\omega_i \beta_i I_{i,0} - \frac{128}{7293r} I_{i,1} - \frac{896}{21\,879r} I_{i,3}$$

$$- \frac{112}{1105r} I_{i,5} + \frac{128}{17r} I_{i,7} - \beta_i I_{i,8} - \frac{9}{r} I_{i,9} \tag{19j}$$

$$\frac{dI_{i,10}}{dr} = -\frac{1792}{230\,945r} I_{i,0} - \frac{960}{46\,189r} I_{i,2} - \frac{2016}{46\,189r} I_{i,4} - \frac{168}{1615r} I_{i,6} + \frac{162}{19r} I_{i,8} - \beta_i I_{i,9} - \frac{10}{r} I_{i,10} \quad (19k)$$

$$\frac{dI_{i,11}}{dr} = \frac{1}{11}\omega_i\beta_i I_{i,0} - \frac{512}{46\,189r} I_{i,1} - \frac{3200}{138\,567r} I_{i,3} - \frac{192}{4199r} I_{i,5} - \frac{240}{2261r} I_{i,7} + \frac{200}{21r} I_{i,9} - \beta_i I_{i,10} - \frac{11}{r} I_{i,11},$$

$$i = 1,2 \quad (19l)$$

where $I_{i,n}(r)$ is defined as

$$I_{i,n}(r) = \int_{\theta=0}^{\pi}\int_{\phi=0}^{2\pi} I_i(r,\theta,\phi)\,(\sin\theta\cos\phi)^n \sin\theta\,d\phi\,d\theta. \quad (20)$$

The boundary conditions for equation (19) are obtained by applying the Marshak approach [8, 23].

Equation (19), with Marshak's boundary conditions, can be adapted to linear two-point boundary-value problems. They are solved by the finite difference method. For the largest optical thickness considered ($\tau_1 = \tau_2 = 5$), a uniform grid of 50 divisions is used. Solutions of a lower-order P-N approximation may be obtained by a similar process.

Obtaining $I_{i,n}(r)$, the hemispherical–hemispherical reflectivity considered in the P-N approximations can be determined from the expression

$$R = 1 + I_{2,1}(r_2). \quad (21)$$

3. RESULTS AND DISCUSSION

The hemispherical–hemispherical reflectivity for various scattering albedos is presented in Table 1(a) for $D_1 = 1.1$, $D_2 = 1.2$ and $\tau_1 = \tau_2 = 0.1$, Table 1(b) for $D_1 = 2$, $D_2 = 3$ and $\tau_1 = \tau_2 = 1$, and Table 1(c) for $D_1 = 6$, $D_2 = 11$ and $\tau_1 = \tau_2 = 5$. Here, the optical thicknesses τ_1 and τ_2 are defined by $\beta_1(r_1 - r_0)$ and $\beta_2(r_2 - r_1)$, respectively. Numerical results are obtained by the collocation method to the exact integral equations and the P-N approximations. As shown in Tables 1(a)–(c), the convergence of the solutions appears as $J_1 = J_2$ and N increase. Since the results for the present problem seem to be unavailable in the literature, comparisons between the results obtained by the two methods are made to examine the correctness of the present analysis. The comparisons show that the agreement between the higher order results of the integral equation method and those of the P-N approximations is excellent, except the results for small scattering albedos or small optical thicknesses.

Moreover, Tables 1(a)–(c) show that the convergent rate of the polynomial expansions of the source function in the integral equation method is rapid for optically thin cases. The discrepancy between the results of the four-term expansion and those of higher order expansions is quite small for a wide range of optical thicknesses and scattering albedos. With a view to engineering applications, it is sufficient to use the four-term expansion ($J_1 = J_2 = 4$). The CPU time required to solve the integral equations depends on the number of expansion terms. Typical run times are about 3.3 min for the cases with $J_1 = J_2 = 4$ and about 102.5 min for the cases with $J_1 = J_2 = 20$ on an AT 486-33 personal computer.

Similar to the one-layer cylindrical problem [15] and the multi-layer planar problem [7], the P-N approximations of low order generate accurate enough results only for the cases with large scattering albedos and large optical thicknesses, as shown in Tables 1(a)–(c). Because the curvature effects make the angular distribution of the intensity more anisotropic for cylindrical geometries, the results of the P-N approximations for two-layer cylindrical media are not so accurate as those for two-layer planar media presented in ref. [7]. For the same reason, when the optical thickness $\tau_1 + \tau_2 = 2\tau_2$ is fixed, the P-N approximations generate better results for the cases with smaller radius ratios. Besides, the CPU time required to solve the P-N approximations depends on the scattering albedo, the optical thickness and the order of approximation. Typical run times are about 7 s for the cases with $\omega_1 = \omega_2 = 0.2$ and $\tau_1 = \tau_2 = 1$ by the P-3 approximation and about 10 min for the cases with $\omega_1 = \omega_2 = 0.995$ and $\tau_1 = \tau_2 = 5$ by the P-11 approximation.

Next, to show the effects of various parameters, Tables 2–4, obtained by the 10-term expansion of the source function ($J_1 = J_2 = 10$), and Table 5, obtained by the P-11 approximation, are presented. Graphic results are also presented.

Each of Tables 1(a)–(c) and 2 reveals that the hemispherical–hemispherical reflectivity R increases with increasing ω_1 for fixed ω_2 and optical thicknesses. A similar tendency can be observed by increasing ω_2 for fixed ω_1 and optical thicknesses. An examination of Tables 1(a)–(c) reveals that the increase of R as ω_2 varies from 0.2 to 0.995 for fixed ω_1 is larger than the increase of R as ω_1 varies from 0.2 to 0.995 for fixed ω_2. That is, the outer layer has a strong influence on R. This tendency is consistent with the definition of R, equation (17). Moreover, when the optical thickness of the outer layer is large, the influence of the inner layer on R is quite minor, as shown in Table 1(c).

Table 2 shows the effects of various combinations of τ_1 and τ_2 on the hemispherical–hemispherical reflectivity R of a medium with a fixed optical thickness $\tau_1 + \tau_2$ for various scattering albedos. We find that for the cases with small ω_2, the reflectivity R increases with the decrease of τ_2. However, for the cases in which ω_2 is very large ($\omega_2 = 0.995$) and far larger than ω_1, the reflectivity R decreases with τ_2; for the cases in which ω_2 is large but not larger than ω_1, the reflectivity R increases with the decrease of τ_2.

Before considering the reflectivity R further, it is worth considering the two constituents, R_c due to

Table 1. Hemispherical–hemispherical reflectivity obtained by the integral equation method and the P-N approximations for $D_1 = 1.1$, $D_2 = 1.2$ and $\tau_1 = \tau_2 = 0.1$ (a), for $D_1 = 2$, $D_2 = 3$ and $\tau_1 = \tau_2 = 1$ (b), and for $D_1 = 6$, $D_2 = 11$ and $\tau_1 = \tau_2 = 5$ (c)

(a)		Integral equation method ($J_1 = J_2$)				P-N approximations		
ω_1	ω_2	$J_1 = 1$	$J_1 = 2$	$J_1 = 4$	$J_1 = 6$	P-1	P-3	P-11
0.2	0.2	0.09241	0.09279	0.09275	0.09275	0.05973	0.07515	0.08967
0.8	0.2	0.13249	0.13249	0.13262	0.13263	0.10117	0.11690	0.12946
0.995	0.2	0.14751	0.14716	0.14741	0.14743	0.11569	0.13174	0.14393
0.2	0.8	0.16323	0.16399	0.16400	0.16399	0.11997	0.14278	0.16463
0.8	0.8	0.21041	0.21102	0.21114	0.21114	0.16714	0.19192	0.21194
0.995	0.8	0.22819	0.22849	0.22873	0.22874	0.18373	0.20949	0.22925
0.2	0.995	0.19001	0.19055	0.19067	0.19067	0.14119	0.16732	0.19246
0.8	0.995	0.24003	0.24048	0.24070	0.24071	0.19048	0.21930	0.24275
0.995	0.995	0.25892	0.25908	0.25942	0.25943	0.20784	0.23792	0.26119
(b)		Integral equation method ($J_1 = J_2$)				P-N approximations		
ω_1	ω_2	$J_1 = 2$	$J_1 = 4$	$J_1 = 8$	$J_1 = 10$	P-1	P-3	P-11
0.2	0.2	0.07996	0.07931	0.07915	0.07914	0.04478	0.06221	0.06760
0.8	0.2	0.09613	0.09542	0.09528	0.09527	0.05857	0.07778	0.08435
0.995	0.2	0.10701	0.10694	0.10682	0.10682	0.06676	0.08830	0.09628
0.2	0.8	0.38090	0.37893	0.37862	0.37861	0.35814	0.36970	0.37183
0.8	0.8	0.43786	0.43380	0.43345	0.43344	0.41958	0.42619	0.42832
0.995	0.8	0.48060	0.47717	0.47688	0.47686	0.46109	0.46865	0.47286
0.2	0.995	0.58267	0.58897	0.58895	0.58894	0.55590	0.58063	0.58369
0.8	0.995	0.69000	0.69462	0.69457	0.69457	0.67482	0.69066	0.69178
0.995	0.995	0.77769	0.78545	0.78553	0.78553	0.76275	0.78088	0.78443
(c)		Integral equation method ($J_1 = J_2$)				P-N approximations		
ω_1	ω_2	$J_1 = 2$	$J_1 = 4$	$J_1 = 10$	$J_1 = 20$	P-1	P-3	P-11
0.2	0.2	0.03095	0.05093	0.05058	0.05048	†	0.03670	0.04633
0.8	0.2	0.03095	0.05093	0.05058	0.05048	†	0.03670	0.04633
0.995	0.2	0.03095	0.05093	0.05058	0.05049	†	0.03670	0.04633
0.2	0.8	0.30329	0.36728	0.36407	0.36384	0.34659	0.35957	0.36217
0.8	0.8	0.30358	0.36751	0.36426	0.36402	0.34673	0.35977	0.36235
0.995	0.8	0.30428	0.36798	0.36466	0.36443	0.34699	0.36018	0.36276
0.2	0.995	0.80470	0.81825	0.81817	0.81811	0.81382	0.81725	0.81772
0.8	0.995	0.82041	0.83471	0.83434	0.83427	0.83188	0.83377	0.83396
0.995	0.995	0.89109	0.89696	0.89715	0.89707	0.89532	0.89664	0.89692

† The datum is negative.

the attenuated incident intensity and R_m due to the radiation scattered by the media.

From the definition $R_c = q_{2c}^{+}(r_2)$ and equation (16a), we find that R_c is independent of the scattering albedos. The dependence of R_c on D_1, D_2, τ_1 and τ_2 is shown in Tables 3(a) and (b). The R_c will approach zero as D_1 and D_2 become close to unity, as shown in Tables 3(a) and (b). It is also found that R_c increases with $\cos^{-1}(1/D_2)$ and $\cos^{-1}(D_1/D_2)$. Table 3(a) shows that R_c decreases with the increase of $\tau_1+\tau_2$ for the situations where D_1 and D_2 are fixed and $\tau_1 = \tau_2$. Table 3(b) reveals that the thinner the τ_2, the larger the R_c for the situations where $\tau_1+\tau_2$ is fixed.

The variation of R_m with various parameters can be found from Table 4. Because the radiation obstructed by the inner opaque cylinder increases with the decrease of D_1 and D_2, R_m decreases as D_1 and D_2 decrease. The combined effects of D_1, D_2 and $\tau_1+\tau_2$ on R_m are also investigated. Because of the mixed influence of the obstruction of radiation and optical thicknesses, the R_m of the media with $\omega_1 = \omega_2$ and fixed D_1 and D_2 increases, reaches a maximum, and then decreases with the increase of $\tau_1+\tau_2 = 2\tau_2$, especially for the cases with large D_1 and D_2. Besides, the optical thickness $\tau_1+\tau_2 = 2\tau_2$, at which the maximum of R_m appears, increases with the increase of $\omega_1 = \omega_2$. The tendency is different from that for radiative transfer in planar composites, in which $R_m = R$ increases with optical thicknesses monotonously. For two-layer cylindrical media with $\omega_1 \neq \omega_2$ and fixed D_1 and D_2, the variation of R_m with respect to $\tau_1+\tau_2 = 2\tau_2$ is similar to what happens in media with $\omega_1 = \omega_2$. However, the optical thickness at which the maximum of R_m appears for the cases with small ω_1 and large ω_2 is larger than that for the cases with large ω_1 and small ω_2, as shown in Fig. 2.

Table 2. Hemispherical–hemispherical reflectivity of a medium with $D_1 = 2$, $D_2 = 3$ and $\tau_1+\tau_2 = 2$

		Optical thickness combination				
ω_1	ω_2	$\tau_1 = 0.4$ $\tau_2 = 1.6$	$\tau_1 = 0.8$ $\tau_2 = 1.2$	$\tau_1 = 1$ $\tau_2 = 1$	$\tau_1 = 1.2$ $\tau_2 = 0.8$	$\tau_1 = 1.6$ $\tau_2 = 0.4$
0.2	0.2	0.06239	0.07115	0.07914	0.09195	0.15225
0.5	0.2	0.06350	0.07476	0.08516	0.10189	0.17948
0.8	0.2	0.06498	0.08046	0.09527	0.11935	0.22984
0.995	0.2	0.06623	0.08644	0.10682	0.14088	0.30008
0.2	0.5	0.17565	0.18490	0.19236	0.20319	0.24650
0.5	0.5	0.17799	0.19133	0.20226	0.21824	0.28085
0.8	0.5	0.18116	0.20173	0.21923	0.24514	0.34508
0.995	0.5	0.18391	0.21291	0.23917	0.27923	0.43632
0.2	0.8	0.38334	0.38044	0.37861	0.37640	0.37133
0.5	0.8	0.39059	0.39520	0.39842	0.40256	0.41671
0.8	0.8	0.40081	0.42003	0.43344	0.45077	0.50288
0.995	0.8	0.41007	0.44828	0.47686	0.51478	0.62863
0.2	0.995	0.67825	0.61949	0.58894	0.55592	0.47711
0.5	0.995	0.70148	0.65194	0.62605	0.59810	0.53328
0.8	0.995	0.73639	0.70963	0.69457	0.67852	0.64150
0.995	0.995	0.77038	0.78038	0.78553	0.79141	0.80332

The combined effects of radius ratios, optical thicknesses and scattering albedos on R may be found by comparing R_c in Table 3(a) and R_m in Table 4. The comparison shows that R_c may be larger than R_m for the cases with small albedos ($\omega_1 = \omega_2 = 0.2$), large D_1 and D_2 and small optical thicknesses. Since R_c/R may be larger than R_m/R for the cases with small scattering albedos and R_c is determined by D_1, D_2, τ_1 and τ_2, the effects of D_1, D_2, and $\tau_1+\tau_2 = 2\tau_2$ on $R = R_c+R_m$ are significant for cases with small scattering albedos.

In the current model, the behaviour of radiative transfer in a two-layer cylindrical medium where the radius ratios are very close to unity is similar to that in a planar medium with the same optical thickness. Thus, for comparison purposes the exact results for planar media [4] are also shown in Table 4. As seen from the table, when the radius ratios approach unity, R_m of a cylindrical medium approaches R of a planar medium with the same optical thickness.

In the limit that the radii become extremely large, the cylindrical system will approximate a planar system. Table 5 shows the limiting process for R obtained by the P-11 approximation. Comparisons of the present results for very large radii and those from ref. [7] for planar systems show good agreement.

Table 3. R_c of a medium with $\tau_1 = \tau_2$ and decreasing radius ratios (a), and R_c of a medium with $\tau_1+\tau_2 = 2$ and decreasing radius ratios (b)

(a)		Optical thickness $\tau_1+\tau_2$			
D_1	D_2	0.1	0.5	2	5
6	11	0.73835	0.34730	0.04376	0.00635
2	3	0.51741	0.21104	0.02232	0.00337
1.5	2	0.37048	0.13153	0.01219	0.00189
1.1	1.2	0.09788	0.01907	0.00131	0.00021
1.05	1.1	0.04457	0.00604	0.00039	0.00006
1.01	1.02	0.00474	0.00029	0.00002	
1.005	1.01	0.00151	0.00007		
1.001	1.002	0.00007			

(b)		Optical thickness combination			
D_1	D_2	$\tau_1 = 0.4$ $\tau_2 = 1.6$	$\tau_1 = 0.8$ $\tau_2 = 1.2$	$\tau_1 = 1.2$ $\tau_2 = 0.8$	$\tau_1 = 1.6$ $\tau_2 = 0.4$
6	11	0.01902	0.03184	0.06303	0.15290
2	3	0.00935	0.01590	0.03321	0.09020
1.5	2	0.00494	0.00857	0.01856	0.05525
1.1	1.2	0.00051	0.00091	0.00204	0.00765
1.05	1.1	0.00015	0.00027	0.00061	0.00238
1.01	1.02	0.00001	0.00001	0.00003	0.00011

Table 4. R_m of a medium with $\tau_1 = \tau_2$ and decreasing radius ratios

				Optical thickness $\tau_1+\tau_2$ ($\tau_1 = \tau_2$)			
ω_1	ω_2	D_1	D_2	0.1	0.5	2	5
0.2	0.2	6	11	0.03107	0.07397	0.06199	0.05179
		2	3	0.02848	0.06447	0.05682	0.05025
		1.5	2	0.02646	0.05806	0.05380	0.04922
		1.1	1.2	0.02079	0.04453	0.04849	0.04725
		1.05	1.1	0.01876	0.04121	0.04738	0.04681
		1.01	1.02	0.01590	0.03801	0.04633	
		1.005	1.01	0.01532	0.03759		
		1.001	1.002	0.01477			
				0.01462†	0.03715†	0.04607†	0.04626†
0.8	0.2	6	11	0.05670	0.13449	0.08057	0.05231
		2	3	0.05614	0.12414	0.07295	0.05072
		1.5	2	0.05478	0.11552	0.06867	0.04967
		1.1	1.2	0.04738	0.09253	0.06138	0.04767
		1.05	1.1	0.04377	0.08591	0.05989	0.04723
		1.01	1.02	0.03804	0.07915	0.05848	
		1.005	1.01	0.03676	0.07819		
		1.001	1.002	0.03546			
				0.03521†	0.07727†	0.05816†	0.04668†
0.2	0.8	6	11	0.10575	0.30953	0.39178	0.37884
		2	3	0.09297	0.26308	0.35629	0.36638
		1.5	2	0.08396	0.23368	0.33632	0.35838
		1.1	1.2	0.06214	0.17627	0.30221	0.34324
		1.05	1.1	0.05520	0.16303	0.29516	0.33974
		1.01	1.02	0.04614	0.15053	0.28804	
		1.005	1.01	0.04440	0.14882		
		1.001	1.002	0.04279			
				0.04230†	0.14723†	0.28698†	0.33591†
0.8	0.8	6	11	0.13385	0.39939	0.45653	0.38614
		2	3	0.12319	0.35021	0.41112	0.37297
		1.5	2	0.11488	0.31708	0.38659	0.36469
		1.1	1.2	0.09123	0.24583	0.34580	0.34916
		1.05	1.1	0.08264	0.22791	0.33752	0.34559
		1.01	1.02	0.07054	0.21034	0.32910	
		1.005	1.01	0.06805	0.20786		
		1.001	1.002	0.06563			
				0.06498†	0.20560†	0.32795†	0.34168†

†The datum is the R obtained by the P-N method [4] for a planar medium with the same optical thickness.

Besides, when $r_2-r_1 = r_1-r_0$ and $\tau_1 = \tau_2$ are fixed, the limit where the radii become large corresponds to the limit where the radius ratios approach unity, as shown in Table 5. Thus, as seen from Table 5, the limiting process of radius ratios to unity has the same effects as the increase of radii.

The hemispherical–directional reflectivity ρ_θ of a cylindrical medium is different from that of a planar medium, because the latter depends only on the polar angle. Thus, it is of interest to investigate the angular dependence of ρ_θ and the influence of various parameters on ρ_θ. Besides, since the attenuated incident radiative intensity plays an important role in the present problem, $\rho_{\theta c}$ is also presented. In Figs. 3(a)–(d), the variation of ρ_θ and $\rho_{\theta c}$ with respect to η are shown on the view planes with $\xi = 0$, $\pi/4$ and $\pi/2$, where each view plane, such as QVP in Fig. 1(a), is defined by the r-axis and a line normal to the r-axis, η is the angle between the r-axis and the leaving intensity $I(r_2, \theta, \phi)$, and ξ is the angle between the plane rVz and a view plane, such as QVP in Fig. 1(a). The relation between (ξ, η) and (θ, ϕ) is $\tan\eta = 1/(\cos\xi \tan\theta \cos\phi)$. The view plane with $\xi = 0$ is a special one, where the attenuated incident radiation does not have direct influence on ρ_θ, and, thus, $\rho_{\theta c} = 0$. Moreover, when $\eta < \eta_s = \tan^{-1}[1/(\cos\xi \tan\theta \cos\phi)]$ with $\phi = \sin^{-1}(1/D_2)$, the attenuated incident radiation is obstructed by the inner opaque cylinder. Thus, on each view plane, $\rho_{\theta c} = 0$ as $\eta < \eta_s$, ρ_θ has a sudden variation at η_s, and both ρ_θ and $\rho_{\theta c}$ increase with the increase of η, as shown in Figs. 3(a)–(d). On the view plane with $\xi \neq 0$, once η reaches $\pi/2$, $\rho_\theta = \rho_{\theta c} = 1/\pi$. When $\eta > \eta_s$, the increase of $\rho_{\theta c}$ with ξ is due to the decrease of the optical path and the increase of ρ_θ with ξ is due to the increase of $\rho_{\theta c}$.

Figures 3(a)–(d) also show the effects of ω_1 and ω_2 on ρ_θ and $\rho_{\theta c}$. Similar to R_c, the scattering albedos do not have any influence on $\rho_{\theta c}$. Besides, when ω_2

Table 5. Hemispherical–hemispherical reflectivity of cylindrical systems with increasing radii and fixed optical thicknesses

ω_1	ω_2	r_0†	r_1†	r_2†	D_1	D_2	Optical thickness $\tau_1 = \tau_2$: 1	5
0.2	0.2	1	2	3	2	3	0.06760	0.04562
		2	3	4	1.5	2	0.05702	0.04523
		10	11	12	1.1	1.2	0.04588	0.04464
		20	21	22	1.05	1.1	0.04494	0.04453
		100	101	102	1.01	1.02	0.04434	0.04443
							0.04421‡	0.04440‡
0.8	0.2	1	2	3	2	3	0.08435	0.04562
		2	3	4	1.5	2	0.07225	0.04523
		10	11	12	1.1	1.2	0.05884	0.04464
		20	21	22	1.05	1.1	0.05749	0.04453
		100	101	102	1.01	1.02	0.05652	0.04443
							0.05629‡	0.04440‡
0.2	0.8	1	2	3	2	3	0.37183	0.35611
		2	3	4	1.5	2	0.34353	0.35216
		10	11	12	1.1	1.2	0.30163	0.34474
		20	21	22	1.05	1.1	0.29431	0.34313
		100	101	102	1.01	1.02	0.28802	0.34164
							0.28638‡	0.34123‡
0.8	0.8	1	2	3	2	3	0.42832	0.35629
		2	3	4	1.5	2	0.39487	0.35234
		10	11	12	1.1	1.2	0.34553	0.34491
		20	21	22	1.05	1.1	0.33688	0.34330
		100	101	102	1.01	1.02	0.32941	0.34180
							0.32746‡	0.34140‡

† The unit of r_0, r_1 and r_2 is length, such as metre.
‡ The datum is the R obtained by the P-11 approximation [7] for a planar medium with the same optical thickness.

becomes smaller, the influence of the inner opaque cylinder on ρ_θ becomes less significant. Comparing the four cases shown in Figs. 3(a)–(d), one can find that the influence of ω_1 on ρ_θ is less than that of ω_2 on ρ_θ.

4. CONCLUSIONS

Some conclusions are summarized below for the present analysis: (a) numerical solutions of the exact integral equations by the collocation method are accurate under various conditions, while the low-order P-N approximations work well only for the cases with large scattering albedos and large optical thicknesses. (b) The influence of the outer layer on the reflectivities is stronger than that of the inner layer. (c) When $\tau_1+\tau_2$ is fixed, for cases with small ω_2, the reflectivities increase with the decrease of τ_2, while when ω_2 is very large ($\omega_2 = 0.995$) and far larger than ω_1, the reflectivities decrease with τ_2. (d) Owing to the attenuated incident radiation and the obstruction of radiation by the inner opaque cylinder, the dependence of the hemispherical–hemispherical reflectivity on radius ratios and optical thicknesses is complicated and the hemispherical–directional reflectivity has complicated angular dependence.

In this work, because of the limits of space and resources, the effects of the reflections at the boundaries have not been investigated. However, it is worthwhile extending this work to the cases with Fresnel boundaries or diffusely reflecting boundaries, because the cases have particular physical significance in fibre optics and in the area of determination of thermal properties by the transient hot wire method.

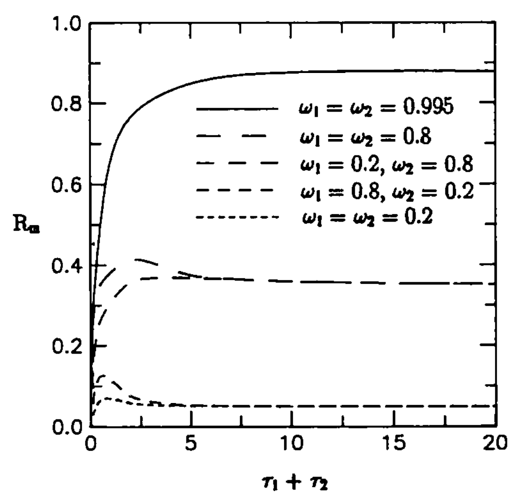

FIG. 2. R_m vs optical thickness, $\tau_1+\tau_2$, for a medium with $D_1 = 2$, $D_2 = 3$ and $\tau_1 = \tau_2$.

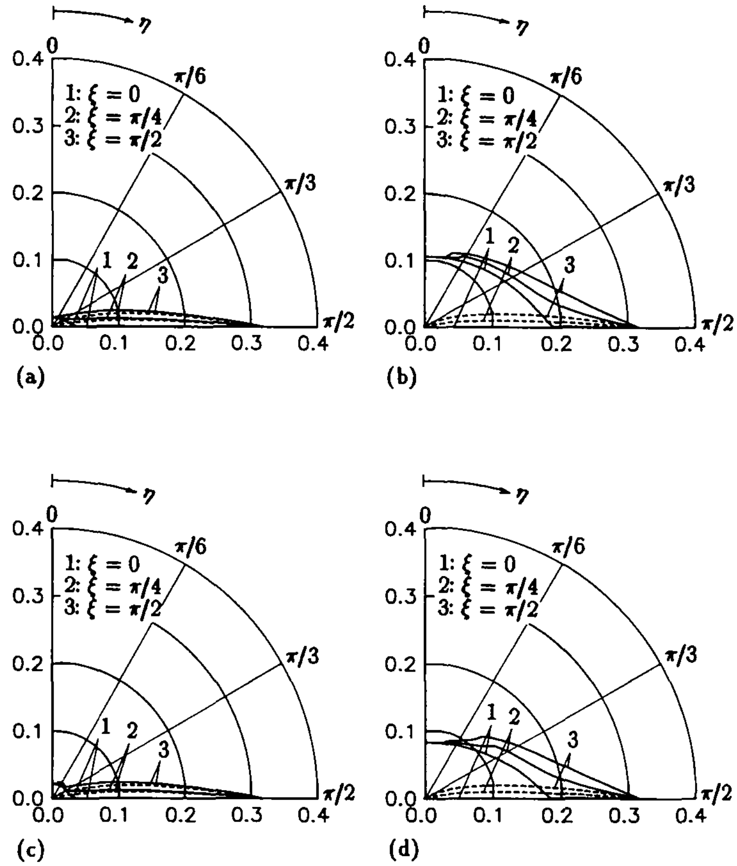

FIG. 3. Reflectivities, ρ_θ (——) and $\rho_{\theta c}$ (----), for a medium with $D_1 = 2$, $D_2 = 3$ and $\tau_1 = \tau_2 = 1$: $\omega_1 = \omega_2 = 0.2$ (a), $\omega_1 = \omega_2 = 0.8$ (b), $\omega_1 = 0.8$, $\omega_2 = 0.2$ (c), and $\omega_1 = 0.2$, $\omega_2 = 0.8$ (d).

Acknowledgement—The authors would like to thank Prof. C. K. Chen for his consideration and encouragement.

REFERENCES

1. S. G. Iliasov and V. V. Krasnikov, Radiation propagation in multi-layer systems with variable optical properties, *Int. J. Heat Mass Transfer* **18**, 769–774 (1975).
2. C. Devaux, P. Grandjean, Y. Ishiguro and C. E. Siewert, On multi-region problems in radiative transfer, *Astrophys. Space Sci.* **62**, 225–233 (1979).
3. S. M. Shouman and M. N. Özisik, Radiative transfer in an isotropically scattering two-region slab with reflecting boundaries, *J. Quant. Spectrosc. Radiat. Transfer* **26**, 1–9 (1981).
4. T. B. Clements and M. N. Özisik, Effects of stepwise variation of albedo on reflectivity and transmissivity of an isotropically scattering slab, *Int. J. Heat Mass Transfer* **26**, 1419–1426 (1983).
5. M. N. Özisik and S. M. Shouman, Source function expansion method for radiative transfer in a two-layer slab, *J. Quant. Spectrosc. Radiat. Transfer* **24**, 441–449 (1980).
6. K. Stamnes and P. Conklin, A new multi-layer discrete ordinate approach to radiative transfer in vertically inhomogeneous atmospheres, *J. Quant. Spectrosc. Radiat. Transfer* **31**, 273–282 (1984).
7. P. S. Swathi, T. W. Tong and G. R. Cunnington, Jr, Reflectance of two-layer composite porous media with linear-anisotropic scattering, *J. Quant. Spectrosc. Radiat. Transfer* **38**, 273–279 (1987).
8. R. Siegel and J. R. Howell, *Thermal Radiation Heat Transfer* (2nd Edn). McGraw-Hill, New York (1981).
9. W. H. Sutton and R. Kamath, Participating radiative heat transfer in a three-dimensional rectangular medium with layered properties, ASME Paper 86-HT-25 (1986).
10. N. M. Reguigui and R. L. Dougherty, Two-dimensional radiative transfer in a cylindrical layered medium with reflecting interfaces, *J. Thermophys.* **6**, 232–241 (1992).
11. C.-H. Ho and M. N. Özisik, Simultaneous conduction and radiation in a two-layer planar medium, *J. Thermophys.* **1**, 154–161 (1987).
12. V. K. Pustovalov and I. A. Khorunzhii, Thermal processes during the interaction of optical radiation pulses with heterogeneous laminated biotissues, *Int. J. Heat Mass Transfer* **33**, 771–783 (1990).
13. M. Perlmutter and J. R. Howell, Radiant transfer through a gray gas between concentric cylinders using Monte Carlo, *J. Heat Transfer* **86C**, 169–179 (1964).
14. S. K. Loyalka, Radiative heat transfer between parallel plates and concentric cylinders, *Int. J. Heat Mass Transfer* **12**, 1513–1517 (1969).
15. Y. Bayazitoğlu and J. Higenyi, Higher-order differential equations of radiative transfer: P-3 approximation, *AIAA J.* **17**, 424–431 (1979).
16. S. T. Thynell and M. N. Özisik, Radiation transfer in absorbing, emitting, isotropically scattering, homogeneous cylindrical media, *J. Quant. Spectrosc. Radiat. Transfer* **38**, 413–426 (1987).
17. A. Kisomi and W. H. Sutton, Source expansion solutions

for radiative transfer in slab, spherical, and cylindrical geometries, *J. Thermophys.* **2,** 370–373 (1988).
18. S. C. Wu and C.-Y. Wu, Partition-extrapolation integration applied to radiative transfer in cylindrical media, *J. Quant. Spectrosc. Radiat. Transfer* **48,** 279–286 (1992).
19. J. R. Tsai and M. N. Özisik, Radiation in cylindrical symmetry with anisotropic scattering and variable properties, *Int. J. Heat Mass Transfer* **33,** 2651–2658 (1990).
20. S. T. Thynell and M. N. Özisik, Integral form of the equation of transfer for an isotropically scattering, inhomogeneous solid cylinder, *J. Quant. Spectrosc. Radiat. Transfer* **36,** 497–503 (1986).
21. W. Squire, Partition-extrapolation methods for numerical quadratures, *Int. J. Comput. Math.* **5,** 81–91 (1975).
22. I. H. Sloan and B. J. Burn, Collocation with polynomials for integral equations of the second kind: a new approach to the theory, *J. Integral Equations* **1,** 77–94 (1979).
23. R. E. Marshak, Note on the spherical harmonics method as applied to the Milne problem for a sphere, *Phys. Rev.* **71,** 443–446 (1947).

APPENDIX

To illustrate the application of the partition-extrapolation technique [18, 21], the second term on the RHS (equation (8b)) having a singularity at $r' = r$ and $\alpha' = 0$ is considered. As an example, we set the singular point to be A and consider only the integration over the domain ABHFE as shown in Fig. 1(b), because of the symmetry to AO. To finish the integration over the domain with the singularity, we partition the domain into two subdomains: one is close to the singularity, ABCD, and the other is far away from the singularity, BHFEDC. The subdomain ABCD close to the singularity is partitioned into many subregions without singularities. Gaussian quadrature is applied to the integration over the subdomain BHFEDC and each subregion of the subdomain ABCD. Then, we apply an extrapolation method to the partial sums of the integrations over the subregions of ABCD repeatedly. Finally, the limit of the process yields the result for the integration over the domain with singularity. The details are similar to those reported in ref. [18].